

## The Influence of Methoxy and Ethoxy Groups on Supramolecular Arrangement of Two Methoxy-chalcones

Jean M. F. Custodio,<sup>a</sup> Eduardo C. M. Faria,<sup>a</sup> Lóide O. Sallum,<sup>a</sup> Vitor S. Duarte,<sup>a</sup>  
 Wesley F. Vaz,<sup>a,b</sup> Gilberto L. B. de Aquino,<sup>a</sup> Paulo S. Carvalho Jr.<sup>a,c</sup> and  
 Hamilton B. Napolitano<sup>\*a</sup>

<sup>a</sup>Campus de Ciências Exatas e Tecnológicas, Universidade Estadual de Goiás,  
 75132-400 Anápolis-GO, Brazil

<sup>b</sup>Instituto Federal de Educação, Ciência e Tecnologia de Mato Grosso,  
 78455-000 Lucas do Rio Verde-MT, Brazil

<sup>c</sup>Instituto de Física de São Carlos, Universidade de São Paulo,  
 CP 369, 13560-970 São Carlos-SP, Brazil

The structures of two methoxylated chalcones, namely (*E*)-1-(4-methoxyphenyl)-3-(3,4,5-trimethoxyphenyl)prop-2-en-1-one and (*E*)-3-(4-ethoxyphenyl)-1-(4-methoxyphenyl)prop-2-en-1-one, reveal the effect of the inclusion of the methoxyl and ethoxyl substituents of the conformation on methoxy-chalcone. Structural comparative study between two chalcones was done in this work and some effects on geometric parameters, such as planarity and dihedral angles, were described. In addition, intermolecular interactions responsible for crystalline packaging were investigated by Hirshfeld surfaces and the values of those interactions were analysed by comparing experimental and theoretical models. The molecular stability was expressed in terms of softness and hardness, both obtained from frontier molecular orbitals. Finally, there is a good agreement between calculated and experimental infrared spectrum, which allowed the assignment of the normal vibrational modes.

**Keywords:** methoxy-chalcones, X-ray diffraction, Hirshfeld surfaces, DFT calculations

### Introduction

Chalcone molecule is a class of flavonoid intermediates that presents pharmacological importance due to their presence in many pharmaceutical compounds.<sup>1-9</sup> Chemically, the molecular skeleton is characterized by aromatic rings moieties connected through three-carbon bridge having a keto carbonyl group and one  $\alpha,\beta$ -unsaturation (Figure 1).<sup>5,10-13</sup>

Chalcones and chalcone derivatives are often obtained from natural or synthetic sources.<sup>8,14</sup> By synthesis perspective, the Claisen-Schmidt condensation of aromatic aldehyde and aromatic acetophenone under either base or acid catalysis is a widely employed method to the synthesis of chalcones.<sup>5,10-13</sup> The versatility of class is evident from its wide-ranging biological activities; in particular, antiviral, anthelmintic, amoebicidal, antibacterial, antiprotozoal, antiulcer, cytotoxic, insecticidal, and anticancer.<sup>13,15-18</sup> Also,

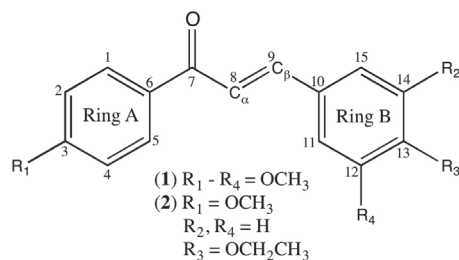


**Figure 1.** Chemical structures of (*E*)-1-(4-methoxy-phen-yl)-3-(3,4,5-trimethoxy-phen-yl)prop-2-en-1-one (1) and (*E*)-3-(4-ethoxyphenyl)-1-(4-methoxyphenyl)prop-2-en-1-one (2).

due to its chemical structure, several chalcones have been reported to exhibit non-linear optical (NLO) properties that turn these compounds into potential functional materials.<sup>19-21</sup> A study with methoxychalcone<sup>19</sup> investigated the optical properties of 3,4-dimethoxy-4'-methoxychalcone and it has shown promise for nonlinear optical applications. On the basis of these features, the investigation on structural and synthetic perspective assumes noteworthy importance for the extending and understanding of the applicability of molecule.

\*e-mail: hbnapolitano@gmail.com

In the course of our studies of chalcone derivatives, we have reported a detailed single crystal analysis for chalcone **2** ((*E*)-3-(4-ethoxyphenyl)-1-(4-methoxyphenyl)prop-2-en-1-one), and a structural comparison with the chalcone **1** ((*E*)-1-(4-methoxyphenyl)-3-(3,4,5-trimethoxyphenyl)prop-2-en-1-one) analogue. The supramolecular and crystal packing features of both structures have been characterized by Hirshfeld surfaces. In addition, electronic structure calculation was performed in order to explain differences due to solid and gas phases, to confirm site of interactions and to evaluate their chemical stability.

## Experimental

### Synthesis and crystallization

It was used 0.3 g (2 mmol) of 4-methoxyacetophenone with 0.39 g (2 mmol) of 3,4,5-trimethoxybenzaldehyde to obtain chalcone **1** and 0.3 g (2 mmol) of 4-methoxyacetophenone with 0.30 g (2 mmol) of 4-ethoxybenzaldehyde benzaldehydes to obtain chalcone **2**. The substituted acetophenones was dissolved in 3 mL of methanol under stirring on ice bath. Then, 9 mL of a NaOH solution (50% m/v) was added after the substituted benzaldehydes. The resulting solution was stirred at room temperature for 24 h and then poured into ice water and neutralized with HCl solution 50%. The resulting precipitate was filtered, washed with water and purified by recrystallization. Chalcone **2** crystallized through slow evaporation of solvent, in which ethyl acetate (CH<sub>3</sub>COOCH<sub>2</sub>CH<sub>3</sub>) was used. The process occurred at 10<sup>th</sup> day at a temperature of 25 °C with bottle semi-open. A yellow prismatic single crystal with dimension of 0.34 × 0.32 × 0.26 mm was selected. Chalcone **1** was also obtained by slow evaporation of solvent, however using methanol (CH<sub>3</sub>OH) as solvent. The crystallization occurred at 5<sup>th</sup> day at a temperature of about 2 °C, with open bottle. For compound **2**, a pale yellow prismatic single crystal measuring 0.59 × 0.515 × 0.445 mm was selected.

### Single crystal X-ray analysis

The diffraction data from chalcone **2** were obtained by the diffractometer KappaCCD model with monochromatic radiation Mo K $\alpha$  at room temperature. Then, the software Saint<sup>22</sup> was used for cell refinement and data reduction. The structure was solved by direct methods and anisotropically refined with full-matrix least-squares on  $F^2$  by the refinement program Shelxl-2014.<sup>23</sup> All the hydrogen atoms were placed in calculated positions and refined with fixed individual displacement parameters

[ $U_{\text{iso}}(\text{H}) = 1.2U_{\text{eq}}$  or  $1.5U_{\text{eq}}$ ] according to the riding model (C–H bond lengths of 0.97 and 0.96 Å, for aromatic and methyl groups, respectively). The Ortep maps from asymmetric unit and the molecular representations were obtained through the programs Ortep,<sup>24</sup> Mercury<sup>25</sup> and Crystal Explorer.<sup>26</sup> The possible H-bond were checked by the Parst<sup>27</sup> and Platon<sup>28</sup> softwares. The crystallographic information files of compound **2** were deposited in the Cambridge Structural Data Base (CCDC)<sup>29,30</sup> under the code CCDC 1529799. Copies of the data can be obtained, free of charge, via [www.ccdc.cam.ac.uk](http://www.ccdc.cam.ac.uk). The compound **1** was previously synthesized and published, under the code CCDC 841293, by our own researcher group<sup>31</sup> and, in order to get a better comparison, those information are also present in Table 1 and Figure 2. Additionally, Table 2 shows the atomic coordinates and equivalent isotropic displacement parameters of compounds **1** and **2**.

**Table 1.** Crystal data and structure refinement for chalcone **1** and chalcone **2**

Parameter	C <sub>19</sub> H <sub>20</sub> O <sub>5</sub> ( <b>1</b> )	C <sub>18</sub> H <sub>18</sub> O <sub>3</sub> ( <b>2</b> )
Formula weight	327.34	282.32
Temperature / K	298 (2)	298 (2)
Wavelength / Å	0.71073	0.71073
Crystal system, space group, Z	monoclinic, P2 <sub>1</sub> /c, 4	orthorhombic, Pna2 <sub>1</sub> , 4
Unit cell dimensions	a = 7.57700 (10) Å b = 16.2530 (5) Å c = 14.0850 (5) Å $\alpha = \gamma = 90^\circ$ $\beta = 107.5280 (10)^\circ$	a = 6.32500 (10) Å b = 14.7150 (3) Å c = 16.2780 (3) Å $\alpha = \beta = \gamma = 90^\circ$
Volume / Å <sup>3</sup>	1654.02 (5)	1515.03 (7)
Calculated density / (mg m <sup>-3</sup> )	1.315	1.238
Absorption coefficient / mm <sup>-1</sup>	0.095	0.083
F (000)	692	600
Refinement method	directed method	directed method
Goodness-of-fit on $F^2$	1.018	1.039
Final R indices [ $I > 2\sigma(I)$ ]	0.0555	0.0540

### Hirshfeld surface analysis

Hirshfeld surface was used to visualize and interpret the potential intermolecular interactions of the compounds in study. The Hirshfeld surface can be understood as an attempt to define the occupied space by a molecule in a crystal where the electronic density is partitioned into molecular fragments and a weight function  $w_a(\mathbf{r})$  is defined for each atom in a molecule as:

$$w_a(\mathbf{r}) = \rho_a^{\text{at}}(\mathbf{r}) / \sum_{i \in \text{molecule}} \rho_i^{\text{at}}(\mathbf{r}) \quad (1)$$

where  $\rho_i^{\text{at}}(\mathbf{r})$  are spherically averaged electron densities of the various atoms. Thus, the electron density of an atomic fragment can be defined as

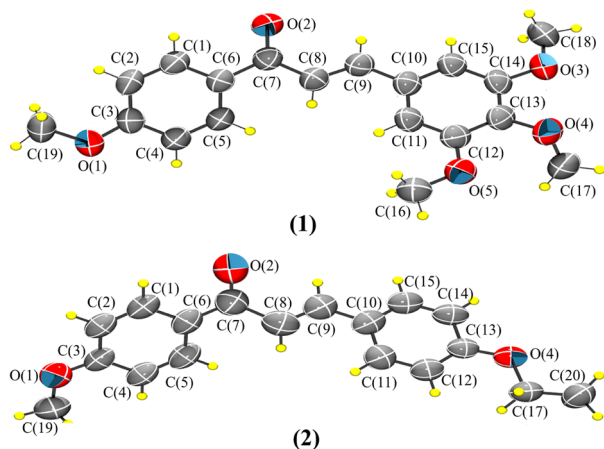


**Figure 2.** Ortep representations with 50% of probability showing numbering scheme for chalcone **1** and **2**.

**Table 2.** Atomic coordinates ( $\times 10^{-4}$ ) and equivalent isotropic displacement parameters ( $\text{\AA}^2 \times 10^3$ ).  $U_{\text{eq}}$  is defined as one third of the trace of the orthogonalized  $U_{ij}$  tensor

Chalcone 1					Chalcone 2				
Atom	x	y	z	$U_{\text{eq}}$	Atom	x	y	z	$U_{\text{eq}}$
O(3)	5650(2)	2234(1)	6370(1)	60(1)	O(2)	-7040(8)	8757(4)	4602(3)	132(2)
O(5)	1609(2)	2627(1)	8267(1)	59(1)	C(19)	-977(9)	9053(6)	834(5)	116(2)
O(1)	7126(2)	200(1)	15087(1)	62(1)	O(4)	976(4)	8776(2)	8708(2)	79(1)
C(6)	7884(2)	197(1)	12291(1)	44(1)	C(13)	-29(6)	8793(2)	7977(3)	68(1)
O(2)	9127(2)	-301(1)	11051(1)	63(1)	C(5)	-2527(7)	9010(3)	3336(3)	85(1)
C(1)	8391(2)	-492(1)	12898(1)	48(1)	C(14)	-1962(6)	9262(3)	7972(3)	80(1)
C(10)	5957(2)	1442(1)	8877(1)	45(1)	C(3)	-3327(7)	8686(2)	1944(3)	75(1)
C(9)	7125(2)	901(1)	9648(1)	47(1)	C(17)	2966(6)	8315(4)	8757(3)	86(1)
O(4)	2518(2)	2803(1)	6546(1)	70(1)	C(12)	689(6)	8382(3)	7259(3)	77(1)
C(3)	7444(2)	158(1)	14187(1)	48(1)	O(1)	-2883(6)	8661(3)	1130(2)	96(1)
C(14)	5303(2)	2063(1)	7249(1)	47(1)	C(1)	-5897(7)	8368(2)	2982(3)	80(1)
C(15)	6421(2)	1569(1)	7999(1)	47(1)	C(8)	-3432(9)	8693(3)	5115(4)	97(1)
C(11)	4386(2)	1820(1)	8996(1)	48(1)	C(11)	-513(7)	8438(3)	6558(3)	83(1)
C(12)	3237(2)	2289(1)	8233(1)	48(1)	C(6)	-4533(7)	8693(3)	3590(3)	80(1)
C(2)	8152(2)	-524(1)	13833(1)	50(1)	C(2)	-5287(7)	8360(2)	2180(3)	79(1)
C(13)	3695(2)	2414(1)	7352(1)	50(1)	C(10)	-2496(7)	8896(3)	6565(3)	83(1)
C(4)	7008(2)	867(1)	13612(1)	53(1)	C(4)	-1933(7)	9016(3)	2533(3)	80(1)
C(7)	8074(2)	183(1)	11269(1)	47(1)	C(7)	-5136(9)	8723(4)	4432(3)	95(1)
C(5)	7205(2)	880(1)	12669(1)	50(1)	C(20)	3802(9)	8455(5)	9605(4)	107(2)
C(8)	6902(2)	757(1)	10531(1)	51(1)	C(15)	-3140(6)	9300(3)	7284(3)	82(1)
C(16)	1014(3)	2440(1)	9115(1)	60(1)	C(9)	-3889(8)	8921(3)	5853(3)	91(1)
C(19)	7389(3)	-528(1)	15679(1)	67(1)					
C(17)	2136(3)	3645(1)	6632(2)	70(1)					
C(18)	7385(3)	1991(1)	6273(1)	70(1)					

$$\rho_a(\mathbf{r}) = w_a(\mathbf{r})\rho^{\text{mol}}(\mathbf{r}) \quad (2)$$

where  $\rho^{\text{mol}}(\mathbf{r})$  indicates the molecular electron density. This graphical tool represents all molecular interactions of a given compound and is important for studying molecular crystal structures because it describes the standards of molecular interactivity and it is possible to estimate the intermolecular contacts that can provide important information of molecular functions. In a Hirshfeld surface the distance from the nearest atoms outside ( $d_e$ ) and inside ( $d_i$ ) the surface and the normalized contact distance based on these,

$$d_{\text{norm}} = (d_i - r_i^{\text{vdw}})/r_i^{\text{vdw}} + (d_e - r_e^{\text{vdw}})/r_e^{\text{vdw}} \quad (3)$$

is symmetric in  $d_e$  and  $d_i$ , with  $r_i^{\text{vdw}}$  and  $r_e^{\text{vdw}}$  being the van der Waals radii of the atoms. In a graphical representation of  $d_{\text{norm}}$ , close intermolecular distances are characterized by two identically colored regions and this function

highlights the donor and acceptor equally and it is therefore a powerful tool for analyzing intermolecular interactions.<sup>32-34</sup>

#### GC-MS analysis

Gas chromatography coupled with mass spectrometry (GC-MS) was carried out on a Shimadzu QP2010-Plus mass spectrometer, in a non-polar columns (RTX-5 Restek, 30 m × 0.25 mm × 0.25 μm film thickness). The column oven was programmed to start at 80 °C for 5 min and subsequently increased to 250 °C at a rate of 20 °C min<sup>-1</sup> with a final hold of 10 min. The chromatogram of **1** (Figure S1) and **2** (Figure S2) are available in the Supplementary Information (SI).

#### Spectroscopic characterization

Infrared spectroscopy (IR), mass spectroscopy and nuclear magnetic resonance of hydrogen (<sup>1</sup>H NMR) (Figures S3 and S4, SI) and carbon (<sup>13</sup>C NMR) (Figures S5 and S6, SI) were carried out. Infrared spectra were recorded on a PerkinElmer Frontier in the range 4000-400 cm<sup>-1</sup> using the KBr pellet technique. <sup>1</sup>H and <sup>13</sup>C NMR spectra were obtained on a Bruker 500 MHz spectrometer using CDCl<sub>3</sub> and MeOD (Aldrich). Chemical shifts assignments were expressed as ppm using tetramethylsilane (TMS) as internal standard. Spectra visualization was performed through the Program ACD LABS 12.0.

#### Chalcone **1**

Yellow powder, m.p. 131.1-132.5 °C; IR (KBr)  $\nu$  / cm<sup>-1</sup> 1612 (C=O); MS:  $m/z$  (%) 328 [M]<sup>+</sup> (100) (C<sub>19</sub>H<sub>20</sub>O<sub>5</sub>); <sup>1</sup>H NMR (500 MHz, CDCl<sub>3</sub>)  $\delta$  3.92 (s, 3H, OCH<sub>3</sub>Ph), 3.93 (s, 3H, OCH<sub>3</sub>Ph), 3.95 (s, 6H, OCH<sub>3</sub>Ph), 6.89 (s, 2H, Ph), 7.02 (d, 2H, *J* 8.85 Hz, PhOCH<sub>3</sub>), 7.44 (d, 1H, *J* 15.56 Hz, CHCO), 7.74 (d, 1H, *J* 15.56 Hz, CHPh), 8.07 (d, 2H, *J* 8.85 Hz, PhOCH<sub>3</sub>); <sup>13</sup>C NMR (126 MHz, CDCl<sub>3</sub>)  $\delta$  OCH<sub>3</sub>Ph (66.46, 66.91, 66.91), Ring Ph (103.29, 104.24, 11.89, 151.54, 159.18, 156.32, 165.31, 167.19), olefin (120.62, 145.10) 170.15 (C=O).

#### Chalcone **2**

Yellow powder, m.p. 101.5-103.2 °C; IR (KBr)  $\nu$  / cm<sup>-1</sup> 1692 (C=O); MS:  $m/z$  (%) 282 [M]<sup>+</sup> (100) (C<sub>18</sub>H<sub>18</sub>O<sub>3</sub>); <sup>1</sup>H NMR (500 MHz, CDCl<sub>3</sub>)  $\delta$  1.46 (t, 3H, *J* 7.0 Hz, CH<sub>3</sub>CH<sub>2</sub>OPh), (s, 3H, OCH<sub>3</sub>Ph), 4.11 (q, 2H, *J* 7.0 Hz, CH<sub>3</sub>CH<sub>2</sub>OPh), 6.97-6.88 (m, 2H), 7.04-6.96 (m, 2H), 7.45 (d, 1H, *J* 15.6 Hz), 7.61 (m, 2H), 7.80 (d, 1H, *J* 15.6 Hz), 8.08-8.01 (m, 2H); <sup>13</sup>C NMR (126 MHz, CDCl<sub>3</sub>)  $\delta$  14.73 (CH<sub>3</sub>CH<sub>2</sub>OPh), 55.47 (OCH<sub>3</sub>Ph), 63.64 (Ar), 113.78,

114.87, 119.47, 127.66, 130.09, 130.68, 131.42, 143.88, 160.93, 163.25, 188.79 (C=O).

#### Computational procedures

For the theoretical calculations it was carried out the molecular geometries of chalcones **1** and **2** from the crystallographic information file (CIF) resulting from the data collection from crystalline samples by means of X-ray diffraction. Then this geometry was fully optimized using the density functional theory (DFT) implemented in the Gaussian 09 package,<sup>35</sup> with the Handy and co-workers<sup>36</sup> long range corrected version of B3LYP using the Coulomb-attenuating method, CAM-B3LYP as functional and, as basis set, we use the 6-311+g(d) of Pople and co-workers.<sup>37</sup> The wavefunction generated using CAM-B3LYP/6-311+g(d) was used for molecular electrostatic potential map (MEP) and frontier molecular orbitals calculations.<sup>38,39</sup>

## Results and Discussion

#### Solid state studies

Obtained solids showed yellow coloration. Compound **1** had a yield of 84%, melting point range: 131.1-132.5 °C. Molecular formula: C<sub>19</sub>H<sub>20</sub>O<sub>5</sub> (328.13 g mol<sup>-1</sup>) while compound **2** had a yield of 99%, melting point range: 101.5-103.2 °C. Molecular formula: C<sub>18</sub>H<sub>18</sub>O<sub>3</sub> (282.13 g mol<sup>-1</sup>).

Since the aromatic substituents have a significant influence on the structure and packing of chalcones, the crystal structure of compounds **1** and **2** have been investigated. Chalcone **1** is a methoxyl-chalcone with three methoxy groups attached to C3, C4 and C5 atoms from ring B. Meanwhile, chalcone **2** presents a similar structure with only one ethoxyl substituent on the ring B (Figures 1 and 2). The compound **1** has crystallized in a monoclinic and space group P2<sub>1</sub>/c, with Z' = 1, while **2**,<sup>31</sup> unlike **1**, crystallized in a orthorhombic crystal system<sup>40</sup> and space group Pna2<sub>1</sub>, also with four molecules *per* unit cell measuring a = 6.32500 (10) Å, b = 14.7150 (3) Å, c = 16.2780 (3) Å and  $\alpha = \beta = \gamma = 90^\circ$ .

From the values obtained by X-ray analysis, it appears that the substituents do not change the bonding distances considerably, since the sum of the differences between all bonds present in both structures is slightly greater than 0.1 Å. About the angles of connection, the greatest difference is found for the angle O1-C3-C4 (8.45°), moreover, there is also a difference of 2.33° in the angle C1-C6-C7. Both mentioned angles are formed

by atoms of ring A. Furthermore, a difference of  $1.88^\circ$  appears for the angle formed by the C10–C15–C14 atoms of ring B, which is the aromatic ring that presents different substituents. Structurally, the difference that attracts the most attention is the difference in the dihedral C19–O1–C3–C4, which causes the methoxy group methyl to be disposed in opposite directions. The experimental and theoretical parameters of chalcones **1** and **2**, obtained by X-ray diffractometry and DFT analysis are present in Table 3.

An overlap (ring A was used as fragment) of chalcones **1** and **2** showed the angle  $\delta$  ( $\delta_1$  for **1** and  $\delta_2$  for **2**) formed between the aromatic rings of the two molecules (Figure 3). This angle is  $36.39^\circ$  for **1** and  $51.18^\circ$  for **2**, occurring in opposite directions in each compound, resulting in a difference of about  $90^\circ$  in relation to plans formed by aromatic A.

When the chalcone **2** is analyzed taking as reference the red plane, it is observed that the molecular planarity deviation arises as expressive form at C8 atom resulting in a value of  $36.39^\circ$  in the aromatic ring. The chalcone **1** on

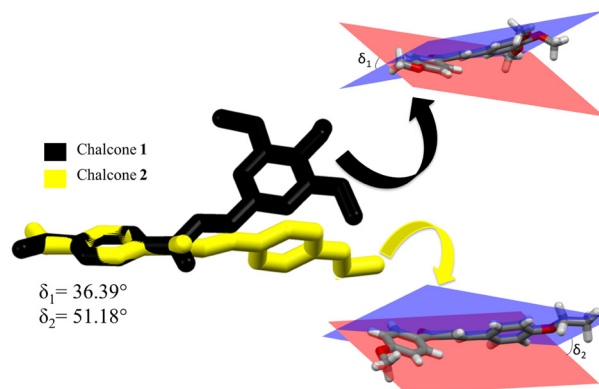


**Figure 3.** Overlapping of **1** and **2**, showing the angles formed by aromatic A (red) and B (blue) rings.

the other hand, although having a deviation of molecular planarity in an opposite direction, also starts the rotation at C8 carbon. Chalcones **1** and **2** also differ by dihedral angles C19–O1–C3–C4 ( $\omega_1$ ), C8–C9–C10–C15 ( $\omega_2$ ) and C14–C13–O4–C17 ( $\omega_3$ ). The values of  $\omega_1$  ( $174.65^\circ$  for **1** and  $-5.26^\circ$  for **2**) and  $\omega_3$  ( $-120.16^\circ$  for **1** and  $-179.54^\circ$  for **2**) show that the methyl from methoxy groups and

**Table 3.** The experimental (X-ray) and theoretical (DFT) geometric parameters of chalcones **1** and **2**

	Bond distance / Å					Bond angle / degree			
	Chalcone 1		Chalcone 2			Chalcone 1		Chalcone 2	
	X-ray	DFT	X-ray	DFT		X-ray	DFT	X-ray	DFT
C19–O1	1.425	1.413	1.421	1.413	C19–O1–C3	118.07	118.75	119.77	118.75
O1–C3	1.361	1.353	1.355	1.353	O1–C3–C4	115.09	115.93	123.54	124.41
C3–C2	1.388	1.393	1.384	1.397	C4–C3–C2	120.18	119.66	119.86	119.70
C2–C1	1.384	1.385	1.361	1.375	C3–C2–C1	119.18	119.45	121.14	120.04
C1–C6	1.391	1.392	1.397	1.400	C2–C1–C6	121.59	121.64	120.48	121.19
C6–C5	1.394	1.398	1.414	1.390	C1–C6–C5	118.16	118.05	117.38	118.09
C5–C4	1.380	1.397	1.360	1.390	C6–C5–C4	120.98	121.03	122.08	121.44
C4–C3	1.391	1.394	1.390	1.390	C5–C4–C3	119.81	120.13	119.04	119.50
C6–C7	1.489	1.492	1.423	1.492	C1–C6–C7	119.49	117.89	121.82	117.90
C7–O2	1.224	1.218	1.237	1.218	C6–C7–O2	120.83	120.00	118.53	119.81
C7–C8	1.478	1.482	1.549	1.481	O2–C7–C8	121.86	120.94	121.20	121.06
C8–C9	1.325	1.336	1.280	1.337	C7–C8–C9	123.59	120.00	120.59	120.02
C9–C10	1.468	1.462	1.456	1.459	C8–C9–C10	125.57	128.03	127.12	128.12
C10–C15	1.399	1.393	1.374	1.401	C9–C10–C15	119.09	117.76	119.17	118.94
C15–C14	1.393	1.392	1.346	1.378	C10–C15–C14	119.88	120.50	121.76	121.63
C14–C13	1.392	1.395	1.404	1.394	C15–C14–C13	120.60	119.92	120.48	120.03
C13–C12	1.401	1.400	1.392	1.394	C14–C13–C12	119.40	119.47	119.52	119.42
C12–C11	1.389	1.387	1.374	1.385	C13–C12–C11	120.02	120.45	119.39	119.73
C11–C10	1.394	1.396	1.424	1.394	C12–C11–C10	120.52	120.01	120.62	121.75
C12–O5	1.364	1.355	–	–	C13–C12–O5	116.14	115.13	–	–
O5–C16	1.432	1.411	–	–	C12–O5–C16	117.33	118.52	–	–
C13–O4	1.369	1.359	1.349	1.353	C14–C13–O4	118.38	119.96	115.12	116.10
O4–C17	1.411	1.421	1.432	1.421	C13–O4–C17	118.42	115.12	118.16	119.20
C14–O3	1.370	1.353	–	–	C15–C14–O3	124.37	124.37	–	–
O3–C18	1.418	1.412	–	–	C14–O3–C18	117.76	118.46	–	–
C17–C20	–	–	1.492	1.509	O4–C17–C20	–	–	107.31	107.69

**Table 4.** Main observed intermolecular interactions for chalcones **1** and **2**

D–H...A	d(D–H) / Å	d(H...A) / Å	d(D...A) / Å	d(D–H...A) / degree
<b>Chalcone 1</b>				
C9–H9...O2 <sup>i</sup>	0.937	2.504	3.417	164.49
C16–H16A...O2 <sup>ii</sup>	0.962	2.555	3.483	162.21
C1–H1...C12 <sup>ii</sup>	0.930	2.800	3.377	121.19
C18–H18C...O1 <sup>iii</sup>	0.943	2.534	3.333	142.61
C5–H5...C14 <sup>i</sup>	0.967	2.805	3.619	142.27
C5–H5...O3 <sup>i</sup>	0.967	2.625	3.582	170.86
C16–H16C...O4 <sup>i</sup>	0.963	2.602	3.290	128.59
<b>Chalcone 2</b>				
C17–H17A...C15 <sup>iv</sup>	1.076	2.674	3.730	167.06
C17–H17A...C14 <sup>iv</sup>	1.076	2.835	3.724	139.90
C17–H17B...C13 <sup>iv</sup>	1.045	2.762	3.584	135.54

$i = -1 + x, y, z$ ;  $ii = 1 - x, -y, -z$ ;  $iii = x, y, -1 + z$ ;  $iiii = 1 + x, y, z$ ;  $iv = -\frac{1}{2} + x, \frac{1}{2} - y, z$ .

methyl/ethyl from aromatic B have a different orientation, due to reversal of the rotation direction of the dihedral, while  $\omega_2$  (176.70° for **1** and 169.72° for **2**) shows the difference due to aromatic B rotation.

In the packing of compound **1** there are interactions of type C–H...O and C–H...C, while the packing of compound **2** presents only C–H...C interactions. The main interactions among **1** and **2** and their geometric parameters are represented in Figure 4 and Table 4.

For chalcone **1**, two C9–H9...O2, C16–H16A...O2 and C1–H1...C12 interactions form dimers (dimer 1 and dimer 2), increasing the structural stability of the compound [Figures 4(1a) and 4(1b)].

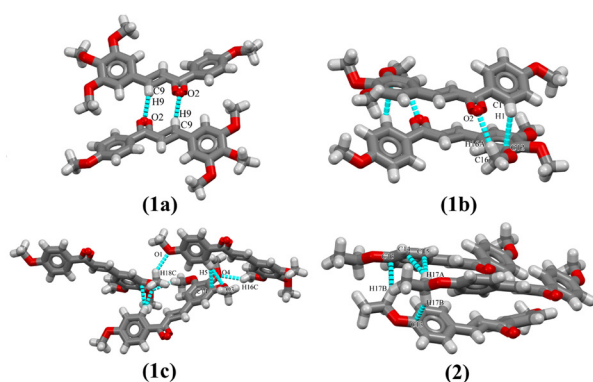


**Figure 4.** Total interactions of chalcone **1** [(1a), (1b) and (1c)] and chalcone **2**. There are two independent dimers in the packing of chalcone **1** [(1a) and 2 (1b)].

The C18–H18C...O1 interaction contributes to the increase in direction of c axis, stacking dimers 1, while C16–H16C...O4, C5–H5...O3 and C5–H5...C14 interactions stack dimers 2 along b and c axis. The interaction C17–H17B...C13 induces the position of

chalcone **2** in b axis direction while the C17–H17A...C15 and C17–H17A...C14 increase the packaging in direction to a and c axis (Figure 4(2)).

By analyzing the Figure 5a, it is possible to see that for the packaging of the first chalcone the angles formed between the molecules and the c axis are bigger (39.19°) than the existing angles in the second molecule that has a most planar layer on packing (4.07°).

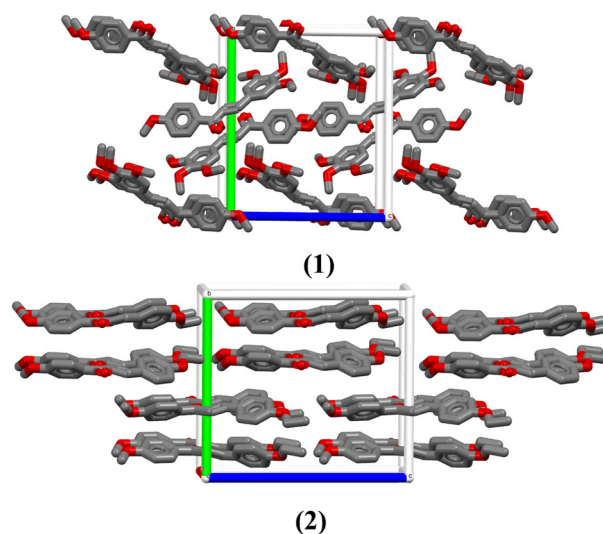


**Figure 5.** Crystal packing of **1** and **2**.

This difference on packing corroborates the non-planarity of compound **1** and hence, the greatest number of intermolecular interactions. It can be explained by the presence of more electronegative group, such as the three methoxy on aromatic ring B. Moreover, the increase on electronegative groups also explains the difference noted

in dihedral angle  $\omega_2$ , present near to carbonyl group and olefinic portion.

The intermolecular interactions of **1** and **2** were visualized and interpreted using Hirshfeld surface (HS) analysis. Hirshfeld surfaces are a valuable tool for the recognition of intermolecular interactions and were used in this study to promote analysis of the intermolecular interactions present in **1** and **2**. First, it involves distances between the nucleus of an internal atom to HS indicating a donor regions of intermolecular contacts ( $d_i$ ), and the distance between an external nucleus to HS indicating an acceptor regions of intermolecular contacts ( $d_e$ ). Then, this surface is denominated  $d_{\text{norm}}$  due to its normalization as a function of van der Waals radius.<sup>34</sup>

Intermolecular interactions of compound **1** are represented in Figures 6(1a) and 6(1b), followed by intermolecular interactions of compound **2**, in Figures 6(2a) and 6(2b), where blue color indicates low intensity and red color indicates high intensity of contacts.

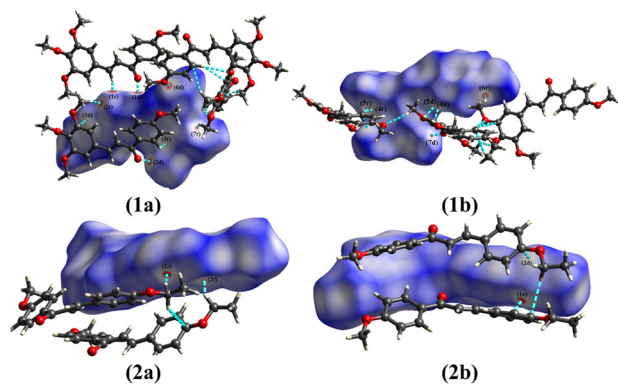


**Figure 6.** Hirshfeld surfaces indicating intermolecular interactions of **1** [(1a) and (1b)] and **2** [(2a) and (2b)].

In chalcone **1**, places indicated by (1r), (2r), (3r), (7r), (4r), (5r) and (6r) are regions of higher  $d_e$  contacts, corresponding to acceptor regions of C9–H9...O2, C16–H16A...O2, C1–H1...C12, C16–H16C...O4, C5–H5...C14, C5–H5...O3 and C18–H18C...O1 interactions, while places indicated by (1d), (2d), (3d), (7d), (4d), (5d) and (6d) are regions of higher  $d_i$  contacts, corresponding to donor regions of these same interactions, respectively. In contrast, for chalcone **2**, acceptor regions of C17–H17A...C15 and C17–H17B...H13 interactions are recognized as red points in (1r) and (2r) in Figure 6(2a), while (1d) and (2d) in Figure 6(2b) represent donor regions of these interactions, with high intensity of  $d_i$ . Note that the places (1r) and (2r) in Figure 6(1a) has a stronger donor character than other places of **1**, while the interaction C17–H17A...C15 is apparently stronger than the interaction C17–H17B...C13 of **2**.

Hirshfeld surfaces also are a great tool for the recognition of hydrophobic interactions ( $\pi\cdots\pi$  and C–H... $\pi$  interactions). The shape index HS expresses important information to understand the three-dimensional arrangement of the compounds studied here. Figure 6 shows the  $\pi$  interactions observed in the crystal packing of **1** and **2**.

Chalcone **1** and chalcone **2** are both stabilized by C–H... $\pi$  interactions (Figure 7). The effect of C–H... $\pi$  interactions from compound **1** involving Cg1 (gravity center of aromatic ring formed by C1, C2, C3, C4, C5 and C6 atoms) are shown in the Figure 7(1), with interaction C19–H19C...Cg1, symmetry code  $2 - x, -y, 1 - z$ , (H19C...Cg1 = 2.83 Å, D–H...A = 144.38°) forming a centrosymmetric dimer.

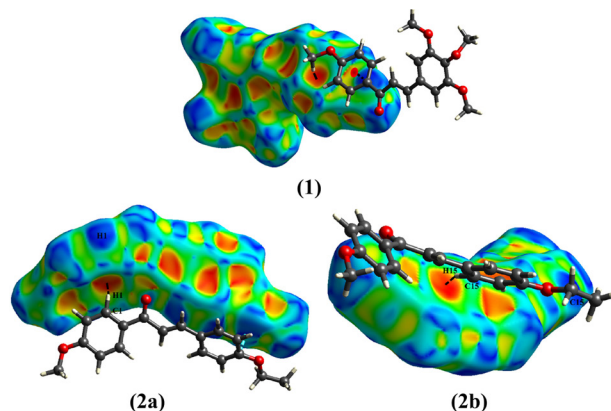


**Figure 7.** Representation of C–H... $\pi$  interactions present in (1), involving C19–H19C...Cg1 and 2a and 2b, involving C1–H1...Cg1 and C15–H15...Cg1. Cg1 is the aromatic ring formed by atoms C1, C2, C3, C4, C5 and C6.

In contrast, chalcone **2** is stabilized by two C–H... $\pi$ , both involving Cg1. The Figures 7(2a) and 7(2b) show interaction C1–H1...Cg1 (symmetry code  $\frac{1}{2} + x, \frac{1}{2} - y, z$ , H1...Cg1 = 2.821 Å, D–H...A = 139.71°) and C15–H15...Cg1 (symmetry code  $1 - x, -y, \frac{1}{2} + z$ , H15...Cg1 = 2.976 Å, D–H...A = 125.54°). Such interactions are indicated by large depressions above aromatic ring and red regions of concave curvature.<sup>41</sup>

The distances  $d_i$  and  $d_e$  were combined on a two-dimensional graph, representing a fingerprint of these functions. This combination of distances functions provides a mapping of all contacts present in the molecule, making the fingerprints unique for each compound.<sup>42</sup> The fingerprints with respective percentage of each contact were established for chalcone **1** and **2** (Figure 8).

In the fingerprints, the C–H... $\pi$  interactions are represented by C...H contacts, while the  $\pi\cdots\pi$  interactions are recognized by C...C contacts. Due to the substitution pattern, **2** has more C–H... $\pi$  interactions than **1**. This

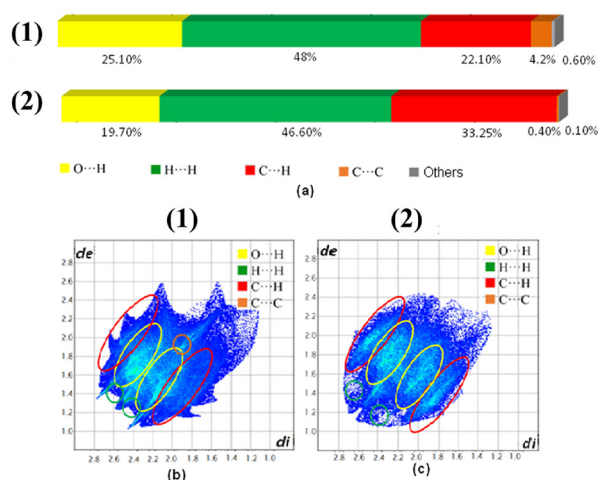


**Figure 8.** Quantification of different types of contacts (a) and the fingerprints established for chalcones **1** and **2** (b and c).

can be explained by the steric hindrance of three methyl groups in **1**. Both structures do not have hydrophobic interactions of the type  $\pi\cdots\pi$  responsible for the crystal packing. The O...H contact represents non-classic hydrogen, representing the C9–H9...O2, C16–H16A...O2, C5–H5...O3, C18–H18C...O1 and C16–H16C...O4 interactions in chalcone **1**. Both compounds are organic molecules, therefore, the interactions index H...H is large; such interactions represent in percentage terms almost half of the total interactions, as indicated in Figure 8a.

#### Theoretical calculations

The root of the mean squared deviation (RMSD) values for internuclear distances and bond angles were calculated for both molecules. It is noted that **1** has a higher difference between theoretical and experimental models ( $\text{RMSD}_1 = 0.3569$ ) than **2** ( $\text{RMSD}_2 = 0.3045$ ), as can be seen in Figure 9.

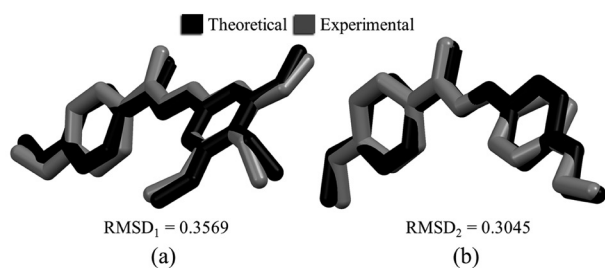


**Figure 9.** Overlapping of theoretical (black) and experimental (gray) models from chalcone **1** (a) and chalcone **2** (b).

Like the deviation of planarity, this higher value for  $\text{RMSD}_1$  is due to stronger intermolecular interactions in **1**. The most variance value for chalcone **1** was observed for the

C7–C8–C9 angle, while C1–C6–C7 is the most variance angle in chalcone **2**. In general, large deviations between these measurements exist because the X-ray results are in the solid phase, while the geometry was optimized for free molecule in vacuum.

MEP is useful for characterizing properties of chemical and biological systems, emphasizing the charge distribution of molecules three-dimensionally.<sup>43</sup> The MEP surface of **2** and **1** are shown in Figure 10. The MEP presents the negative red regions and they are concentrated at the oxygen atoms showing the electrophilic sites of both molecules.

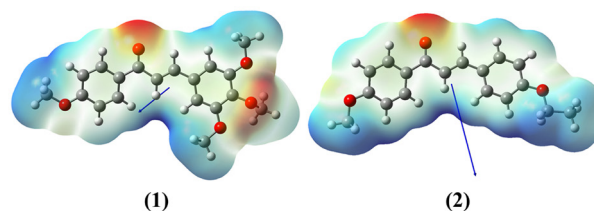


**Figure 10.** Electrostatic potential maps for **1** and **2**. Red color indicates regions more negative.

Blue regions show positive charge concentration areas, which are concentrated over the hydrogen atoms and methyl groups explaining the nucleophile sites of both molecules. The green region represents the zero potential regions. Therefore, when examining the Figure 10 it can be confirmed the existence of intra and intermolecular interactions of these molecules in solid state. The dipole moment is another parameter that predicts the polarized nature of the molecule.<sup>44</sup> The theoretical calculations show that compound **2** (6.2954 D) has more than double of the value of dipole moment of compound **1** (3.0503 D), being the most polarized between the title compounds. We can see that the electron density on the O4 atom is different in the compounds, for chalcone **1** the charge in O4 atom is more negative than the same atom in chalcone **2**.

The difference in energy of the highest occupied molecular orbital (HOMO) and lowest unoccupied molecular orbital (LUMO) orbitals is an important index for the chemical stability of molecules, these energies are directly related to the ability to donate and accept electrons. The energy difference between HOMO and LUMO is an important chemical stability index. A small HOMO-LUMO gap automatically means small excitation energies to the manifold of excited states and a large HOMO-LUMO gap implies high stability with respect to chemical reaction. They are also used to describe chemical softness and hardness.<sup>6,45</sup> The distribution and levels of energy for HOMO and LUMO orbitals for chalcones **1** and **2** were calculated at the theory level CAM-B3LYP/6-311+G(d) (Figure 11). For chalcone **1** the HOMO orbital

is localized entirely on the ring with the trimethoxy group and in the vinyl group, while the LUMO orbital is spread out throughout the molecule, except for two methoxy groups.

For **2** the HOMO and LUMO orbitals are spread out throughout the molecule, except for methyl groups. The high gap energy for chalcone **2** (6.4007 against 6.2611 eV for chalcone **1**) indicates that this compound has a slightly high kinetic stability and low chemical reactivity. The following formulas<sup>46</sup> were used to calculate softness ( $\sigma$ ) and hardness ( $\eta$ ), respectively:

$$\sigma = \frac{-2}{(E_{\text{HOMO}} - E_{\text{LUMO}})} \quad (4)$$

$$\eta = -\frac{1}{2}(E_{\text{HOMO}} - E_{\text{LUMO}}) \quad (5)$$

The softness and hardness were calculated for **2** ( $\sigma = 0.3124$  eV and  $\eta = 3.2003$  eV) and for **1** ( $\sigma = 0.3194$  eV and  $\eta = 3.1305$  eV). Thus we conclude the **1** has a higher capacity to receive electrons while **2** has a higher capacity to resist charge transference (i.e., resistance to change its electronic configuration).

### Assignments

The infrared absorption spectra of chalcones **1** and **2** were obtained in KBr, ca. 1% solution, on FTIR/IR Affinity-1 Shimadzu spectrophotometer, and the principal absorptions bands (4000 to 400  $\text{cm}^{-1}$ ) are represented in Table 5.

Figure 12 shows the theoretical and the experimental infrared spectra of **1** and **2**. As can be seen in Table 5, these values are in line with each other and between the expected experimental values, according to the literature.<sup>47</sup>

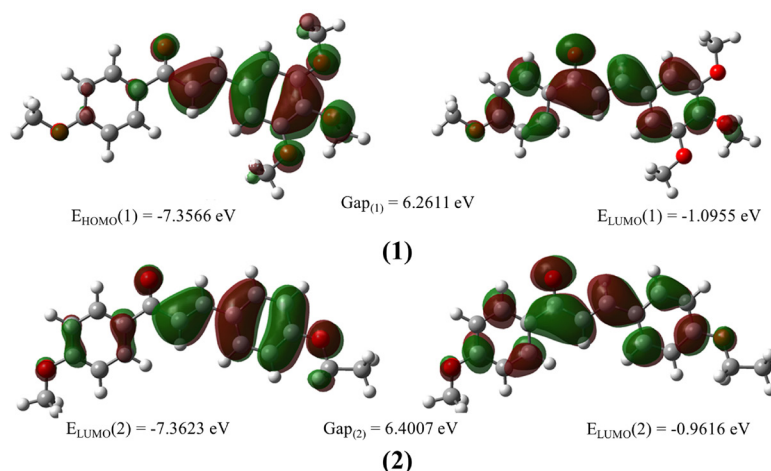


**Figure 11.** Frontier molecular orbitals of chalcones **1** and **2**, followed by calculated homo and lumo band-gaps.

**Table 5.** Vibrational assignments, experimental and calculated wavenumbers in  $\text{cm}^{-1}$  of **1** and **2** at CAM-B3LYP/6-311+g(d)

IR assignments	Unscaled IR frequency <sup>a</sup> / $\text{cm}^{-1}$	Scaled IR frequency <sup>a</sup> / $\text{cm}^{-1}$	I / ( $\text{K mmol}^{-1}$ )	FTIR / ( $\text{K mmol}^{-1}$ )
$\nu(\text{C}=\text{O})$	(1) 1765.20	1691.06	179.32	1612
	(2) 1766.86	1692.65	146.59	1656
$\nu(\text{C}=\text{C})$	(1) 1700.65	1629.22	46.80	1589
	(2) 1695.85	1624.62	586.38	1607
$\nu_{\text{sym}}(\text{CH}_3)$	(1) 3044.19, 3070.54	2916.33, 2941.57	52.61, 24.06	2914, 2948
	(2) 3041.38-3047.98	2913.64-2919.96	47.59-59.83	2840-2927
$\nu_{\text{asym}}(\text{CH}_3)$	(1) 3108.73, 3140.11	2978.16, 3008.22	34.84, 23.42	2967
	(2) 3105.43-3115.88	2975.00-2985.01	33.12-28.89	2944-3000
$\nu(\text{O}-\text{C}_{\text{Aryl}})$	(1) 1338.89, 1304.81	1282.65, 1250.00	56.05, 350.19	1360, 1305
	(2) 1298.90, 1314.90, 1408.16	1244.34, 1259.67, 1349.01	91.72, 391.49, 20.57	1254, 1269, 1332
$\nu(\text{O}-\text{C})$	(1) 1095.97, 1097.86	1049.93, 1051.74	59.68, 65.78	974-1019
	(2) 1071.92-1108.25	1026.89-1061.70	212.72-3.80	996-1029

IR: infrared; I: IR intensities; FTIR: Fourier transform infrared spectroscopy;  $\nu$ : stretching. <sup>a</sup>Scale factor 0.958.

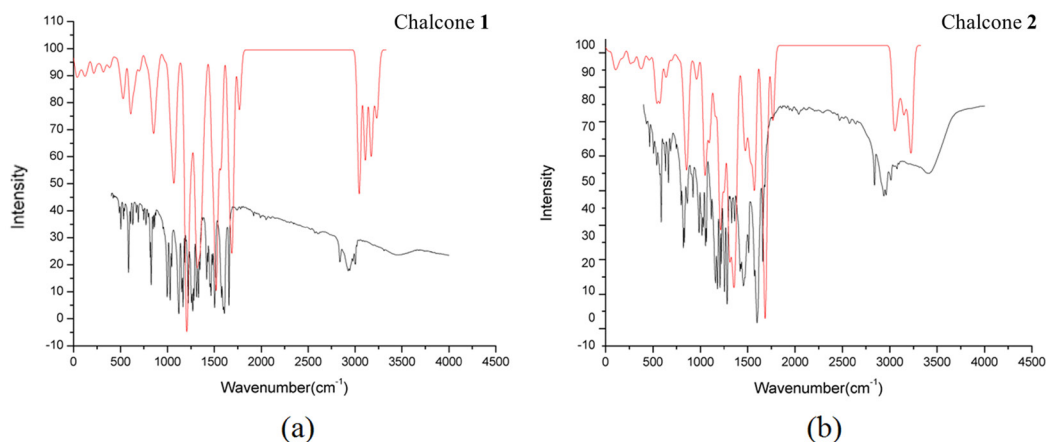


**Figure 12.** Experimental (KBr) (black) and theoretical (red) IR spectra of chalcones **1** and **2**.

In order to make a better comparison between theoretical and experimental results, we apply in the theoretical values a scaling factor of 0.958<sup>48</sup> for the results obtained at CAM-B3LYP/6-311+g(d) level of theory. This procedure corrects the systematic overestimation of the vibrational frequencies that is characteristic of the DFT methods and, besides, makes easier the assignments of the vibrational modes. In this study the IR spectra were obtained for **1** and **2** dissolved in KBr and theoretical measurements were made supposing they were in gas phase, which may explain the difference between results.

Experimentally the carbonyl group strongly absorbs in the range from 1850 to 1650  $\text{cm}^{-1}$ . In chalcones we must consider the conjugations effects that increase the single bond character of the C=O and C=C bonds in the resonance hybrid and hence lower their force constants, resulting in a lowering of the frequencies absorptions. Generally, this effect results in a 25 to 45  $\text{cm}^{-1}$  lowering of the carbonyl frequency.<sup>49</sup> These calculated frequencies are 1691.06  $\text{cm}^{-1}$  for chalcone **2** and 1692.65  $\text{cm}^{-1}$  for chalcone **1**, in experimental IR spectra these values are 1612 and 1656  $\text{cm}^{-1}$ , respectively. For chalcones with methoxy group, just like in both molecules, the C=O stretching occurs, in average, around 1663  $\text{cm}^{-1}$ . The stretching modes of vinyl group occur at 1660-1600  $\text{cm}^{-1}$  though C=C stretch appears at lower frequencies, with increased intensity, when conjugated with carbonyl group.<sup>49</sup> The calculated wavenumbers for this mode are 1629.22 and 1624.62  $\text{cm}^{-1}$  for chalcone **2** and chalcone **1**, respectively, and in the IR spectra these modes appear in 1589 and 1607  $\text{cm}^{-1}$ , respectively. The O–C stretching vibration of the O-CH<sub>3</sub> group appears in the wide region of  $975 \pm 125 \text{ cm}^{-1}$  with an intensity varying from weak to strong.<sup>47,50</sup> The O-CH<sub>3</sub> stretching was calculated at 1049-1051  $\text{cm}^{-1}$  for chalcone **2**, while experimental bands appears in 974-1019  $\text{cm}^{-1}$ . In the range of 1026.89-1061.70  $\text{cm}^{-1}$  for chalcone **1**, it

can be observed as weak bands in IR at 996-1029  $\text{cm}^{-1}$ . A methoxy group attached to an aromatic ring gives the asymmetric stretching in the range 1310-1210  $\text{cm}^{-1}$ .<sup>50</sup> The *ab initio* calculations give 1338.89 and 1304.81  $\text{cm}^{-1}$  as methoxy stretching vibrations for chalcone **2**, while chalcone **1** presents these vibrations in 1244.34, 1259.67 and 1349.01  $\text{cm}^{-1}$ . IR spectra values for this vibrational mode appear in 1360 and 1305  $\text{cm}^{-1}$  for chalcone **2** and 1254, 1269 and 1332  $\text{cm}^{-1}$  for chalcone **1**. Electronic effects such as back-donation and induction, mainly caused by the presence of oxygen atom adjacent to methyl group, can shift the position of CH stretching mode. In aromatic methoxy compounds the asymmetric mode are expected in the regions  $2985 \pm 20$  and  $2955 \pm 20 \text{ cm}^{-1}$  and the symmetric mode in the region  $2845 \pm 15 \text{ cm}^{-1}$ .<sup>50</sup> For chalcone **2** the computed wavenumbers of asymmetric stretching of CH<sub>3</sub> group are 2978.16 and 3008.22  $\text{cm}^{-1}$ , while the bands in 2916.33 and 2941.57  $\text{cm}^{-1}$  are assigned as symmetric stretching mode. In IR spectra these values are 2967  $\text{cm}^{-1}$  for asymmetric stretching and 2914 and 2948  $\text{cm}^{-1}$  as symmetric stretching mode. For chalcone **1** the computed wavenumbers of asymmetric stretching of CH<sub>3</sub> group are in the range of 2975.00-2985.01  $\text{cm}^{-1}$ , while the bands in the range of 2913.64-2919.96  $\text{cm}^{-1}$  are assigned as symmetric stretching mode. In the IR spectra, these values are 2944-3000  $\text{cm}^{-1}$  and 2840-2927  $\text{cm}^{-1}$  for asymmetric and symmetric stretching modes, respectively.

## Conclusions

Different substitution patterns of aromatic B caused significant variations in the crystal structure of the chalcones studied. Chalcone **1**, due to its greater number of methoxy groups, has an increase in its electronegativity and, hence, has more intermolecular interactions than chalcone **2**. These interactions can be the planarity deviation

cause, observed by overlapping of both structure. In contrast, the crystalline state of chalcone **2** is stabilized by only C–H...C and C–H... $\pi$  interactions, as can be seen by the shape index Hirshfeld surfaces.

The theoretical calculations using CAM-B3LYP/6-311+g(d) systematically over-estimated the IR vibrational spectra and to avoid this we used a scale factor<sup>48</sup> of 0.958 with the objective of better convergence with the experimental results. The spectroscopic data are consistent with the crystal structure. Moreover, the CAM-B3LYP functional showed to be a good option to obtain the vibrational spectra. The correlation between the experimental and theoretical structural values is very good, the higher variance value in **1** was observed for the C7–C8–C9 angle while in **2** the C1–C6–C7 angle was the higher variance. With respect to the dipole moment, compound **2** has more than the double of the value of compound **1** which makes it the most polarized molecule between the title compounds. Of the analysis of the frontier molecular orbitals we have that the compound **2** has slightly higher kinetic stability and lower chemical reactivity compared to compound **1**, furthermore, the softness and chemical hardness energy, the results shown compound **1** has a higher capacity to receive electrons while compound **2** has a higher capacity to resist a charge transference.

## Supplementary Information

Supplementary information (GC-MS chromatogram, <sup>1</sup>H NMR and <sup>13</sup>C NMR) is available free of charge at <http://jbcs.sbq.org.br> as PDF file.

## Acknowledgments

The authors are grateful to the Conselho Nacional de Desenvolvimento Científico e Tecnológico (CNPq, grant number 313070/2014-8). Also, the authors are thankful to Fundação de Amparo à Pesquisa do Estado de Goiás for financial support.

## References

1. Bitencourt, H. R.; Guillhon, G. M. S. P.; Arruda, M. S. P.; Marinho, A. M. R.; Santos, A. S.; Brasil, D. S. B.; Santos, L. S.; *J. Braz. Chem. Soc.* **2011**, *22*, 1333.
2. Gaikwad, P.; Priyadarsini, K. I.; Naumov, S.; Rao, B. S. M.; *J. Phys. Chem. A* **2010**, *114*, 7877.
3. Isa, N. M.; Abdelwahab, S. I.; Mohan, S.; Abdul, A. B.; Sukari, M. A.; Taha, M. M. E.; Syam, S.; Narrima, P.; Cheah, S. C.; Ahmad, S.; Mustafa, M. R.; *Braz. J. Med. Biol. Res.* **2012**, *45*, 524.
4. Rafiee, E.; Rahimi, F.; *J. Chil. Chem. Soc.* **2013**, *3*, 2.
5. Sallum, L. O.; Napolitano, H. B.; Carvalho, P. S.; Cidade, A. F.; de Aquino, G. L. B.; Coutinho, N. D.; Camargo, A. J.; Ellena, J.; de Oliveira, H. C. B.; Silva, V. H. C.; *J. Phys. Chem. A* **2014**, *118*, 10048.
6. Vaz, W. F.; Custodio, J. M. F.; Silveira, R. G.; Castro, A. N.; Campos, C. E. M.; Anjos, M. M.; Oliveira, G. R.; Valverde, C.; Baseia, B.; Napolitano, H. B.; *RSC Adv.* **2016**, *6*, 79215.
7. Yerragunta, V.; Kumaraswamy, T.; Suman, D.; Anusha, V.; Patil, P.; Samhitha, T.; *PharmaTutor* **2013**, *1*, 54.
8. Ghosh, R.; Das, A.; *World J. Pharm. Pharm. Sci.* **2014**, *3*, 578.
9. Díaz-Tielas, C.; Graña, E.; Reigosa, M. J.; Sánchez-Moreiras, A. M.; *Planta Daninha* **2016**, *34*, 607.
10. Climent, M. J.; Corma, A.; Iborra, S.; Primo, J.; *J. Catal.* **1995**, *151*, 60.
11. Ritter, M.; Martins, R. M.; Rosa, S. A.; Malavolta, J. L.; Lund, R. G.; Flores, A. F. C.; Pereira, C. M. P.; *J. Braz. Chem. Soc.* **2015**, *26*, 1201.
12. Siddiqui, Z. N.; Khan, T.; *J. Braz. Chem. Soc.* **2014**, *25*, 1002.
13. Silva, W. A.; Andrade, C. K. Z.; Napolitano, H. B.; Vencato, I.; Lariucci, C.; de Castro, M. M. R. C.; Camargo, A. J.; *J. Braz. Chem. Soc.* **2013**, *24*, 133.
14. Bukhari, S. N. A.; Jasamai, M.; Jantan, I.; Ahmad, W.; *Mini-Rev. Org. Chem.* **2013**, *10*, 73.
15. Rando, D. G.; Giarolla, J.; Pasqualoto, K. F. M.; Ferreira, E. I.; *Braz. J. Pharm. Sci.* **2010**, *46*, 311.
16. Matos, M. J.; Vazquez-Rodriguez, S.; Uriarte, E.; Santana, L.; *Expert Opin. Ther. Pat.* **2015**, *25*, 351.
17. Zhai, L.; *J. Antimicrob. Chemother.* **1999**, *43*, 793.
18. Nowakowska, Z.; *Eur. J. Med. Chem.* **2007**, *42*, 125.
19. Shettigar, V.; Patil, P. S.; Naveen, S.; Dharmaprasad, S. M.; Sridhar, M. A.; Shashidhara Prasad, J.; *J. Cryst. Growth* **2006**, *295*, 44.
20. D'silva, E. D.; Podagatlapalli, G. K.; Rao, S. V.; Rao, D. N.; Dharmaprasad, S. M.; *Cryst. Growth Des.* **2011**, *11*, 5362.
21. Prabhu, A. N.; Jayarama, A.; Subrahmanya Bhat, K.; Upadhyaya, V.; *J. Mol. Struct.* **2013**, *1031*, 79.
22. SAINT: Area-Detector Integration Software; Siemens Industrial Automation Inc., Madison, 1995.
23. Sheldrick, G. M.; *Acta Crystallogr. Sect. C* **2015**, *71*, 3.
24. Farrugia, L. J.; *J. Appl. Crystallogr.* **2012**, *45*, 849.
25. Macrae, C. F.; Edgington, P. R.; McCabe, P.; Pidcock, E.; Shields, G. P.; Taylor, R.; Towler, M.; van de Streek, J.; *J. Appl. Crystallogr.* **2006**, *39*, 453.
26. Wolff, S. K.; Grimwood, D. J.; McKinnon, J. J.; Turner, M. J.; Jayatilaka, D.; Spackman, M. A.; *Crystal Explorer (version 3.1)*; University of Western Australia, Crawley, Australia, 2012.
27. Nardelli, M.; *J. Appl. Crystallogr.* **1995**, *28*, 659.
28. Spek, A. L.; *Acta Crystallogr. Sect. D* **2009**, *65*, 148.
29. Groom, C. R.; Allen, F. H.; *Angew. Chem., Int. Ed.* **2014**, *53*, 662.

30. Battle, G. M.; Ferrence, G. M.; Allen, F. H.; *J. Appl. Crystallogr.* **2010**, *43*, 1208.
31. Carvalho-Jr, P. S.; Sallum, L. O.; Cidade, A. F.; Aquino, G. L. B.; Napolitano, H. B.; *Acta Crystallogr. Sect. E Struct. Reports Online* **2011**, *E67*, 0.
32. Soudani, S.; Ferretti, V.; Jelsch, C.; Lefebvre, F.; Ben Nasr, C.; *Inorg. Chem. Commun.* **2015**, *61*, 187.
33. Hirshfeld, F. L.; *Isr. J. Chem.* **1977**, *16*, 198.
34. McKinnon, J. J.; Spackman, M. A.; Mitchell, A. S.; *Acta Crystallogr. Sect. B* **2004**, *60*, 627.
35. Frisch, M. J.; Trucks, G. W.; Schlegel, H. B.; Scuseria, G. E.; Robb, M. A.; Cheeseman, J. R.; Scalmani, G.; Barone, V.; Mennucci, B.; Petersson, G. A.; Nakatsuji, H.; Caricato, M.; Li, X.; Hratchian, H. P.; Izmaylov, A. F.; Bloino, J.; Zheng, G.; Sonnenberg, J. L.; Hada, M.; Ehara, M.; Toyota, K.; Fukuda, R.; Hasegawa, J.; Ishida, M.; Nakajima, T.; Honda, Y.; Kitao, O.; Nakai, H.; Vreven, T.; Montgomery Jr., J. A.; Peralta, J. E.; Ogliaro, F.; Bearpark, M.; Heyd, J. J.; Brothers, E.; Kudin, K. N.; Staroverov, V. N.; Kobayashi, R.; Normand, J.; Raghavachari, K.; Rendell, A.; Burant, J. C.; Iyengar, S. S.; Tomasi, J.; Cossi, M.; Rega, N.; Millam, J. M.; Klene, M.; Knox, J. E.; Cross, J. B.; Bakken, V.; Adamo, C.; Jaramillo, J.; Gomperts, R.; Stratmann, R. E.; Yazyev, O.; Austin, A. J.; Cammi, R.; Pomelli, C.; Ochterski, J. W.; Martin, R. L.; Morokuma, K.; Zakrzewski, V. G.; Voth, G. A.; Salvador, P.; Dannenberg, J. J.; Dapprich, S.; Daniels, A. D.; Farkas, Ö.; Foresman, J. B.; Ortiz, J. V.; Cioslowski, J.; Fox, D. J.; *Gaussian 09, Revision A.02*; Gaussian Inc.: Wallingford CT, 2009.
36. Yanai, T.; Tew, D. P.; Handy, N. C.; *Chem. Phys. Lett.* **2004**, *393*, 51.
37. Krishnan, R.; Binkley, J. S.; Seeger, R.; Pople, J. A.; **1980**, *72*, 650.
38. Fukui, K.; *Science* **1982**, *218*, 747.
39. Foresman, J. B.; Frisch, A.; *Exploring Chemistry with Electronic Structure Methods: A Guide to Using Gaussian*, 2<sup>nd</sup> ed.; Gaussian Inc.: Pittsburgh, USA, 1996.
40. Pauffler, P.; *Acta Crystallogr. Sect. A* **2004**, *60*, 641.
41. Spackman, M. A.; Jayatilaka, D.; *CrystEngComm* **2009**, *11*, 19.
42. Spackman, M. A.; McKinnon, J. J.; *CrystEngComm* **2002**, *4*, 378.
43. Galabov, B.; Nikolova, V.; Ilieva, S.; *Chem. - Eur. J.* **2013**, *19*, 5149.
44. Gece, G.; *Corros. Rev.* **2015**, *33*, 195.
45. Ternavisk, R. R.; Camargo, A. J.; Machado, F. B. C.; Rocco, J. A. F. F.; Aquino, G. L. B.; Silva, V. H. C.; Napolitano, H. B.; *J. Mol. Model.* **2014**, *20*, 2526.
46. Ramagathan, B.; Gopiraman, M.; Olasunkanmi, L. O.; Kabanda, M. M.; Yesudass, S.; Bahadur, I.; Adekunle, A. S.; Obot, I. B.; Ebenso, E. E.; *RSC Adv.* **2015**, *5*, 76675.
47. Raj, A.; Raju, K.; Varghese, H. T.; Granadeiro, C. M.; Nogueira, H. I. S.; Yohannan Panicker, C.; *J. Braz. Chem. Soc.* **2009**, *20*, 549.
48. Barnes, L.; Schindler, B.; Allouche, A.-R.; Simon, D.; Chambert, S.; Oomens, J.; Compagnon, I.; *Phys. Chem. Chem. Phys.* **2015**, *17*, 25705.
49. Pavia, D. L.; Lampman, G. M.; Kriz, G. S.; Vyvyan, J. A.; *Introduction to Spectroscopy*, 5<sup>th</sup> ed.; Cengage Learning: Ohio, USA, 2015.
50. Panicker, C. Y.; Varghese, H. T.; John, M. A.; Harikumar, B.; *Orient. J. Chem.* **2008**, *24*, 973.

Submitted: February 1, 2017

Published online: April 10, 2017